Doctoral Dissertation

# Precise Control of Heart Rate via Closed-Loop Medulla Stimulation and Non-Invasive Cardiac Modulation using Sonogenetics

（閉ループ延髄刺激による心拍数の精密制御と超音波による心機能制御）

XU Yizhou

Graduate School of Life Science, Hokkaido University

2025. 9

# Contents

# Abstract

Cardiovascular diseases are the main cause of global mortality, with autonomic nervous system (ANS) dysregulation as a critical pathophysiology. Traditional pharmaceutical and neuromodulation treatments like vagus nerve stimulation (VNS) face the limitations due to their invasive methos, lack of time-target, and inability to precisely modulate sympathetic-parasympathetic balance. This research investigated the ability of medulla for precise autonomic neuromodulation using heart rate as the index and established a non-invasive method to control medullary sympathetic output.

The systematic investigation of open-loop electrical stimulation in anesthetized Wistar rats (n=24) quantified parameter-response relationships across three targets: rostral ventrolateral medulla (RVLM), caudal ventrolateral medulla (CVLM), and cervical vagus nerve. RVLM stimulation evoked immediate tachycardia with concomitant PR interval shortening while CVLM stimulation induced profound bradycardia without conduction effects. Crucially, I demonstrated frequency dependence as a fundamental factor in electrical stimulation. VNS produced expected bradycardia but with significant PR prolongation. Heart rate variability (HRV) analysis (SDRR, SD1, SD2) confirmed sustained heart rate changes during effective stimulation. Building on parametric characterization, I engineered a real-time closed-loop method implementing a bang-bang control algorithm to maintain HR at specific targets (+20% or -10% of baseline) via RVLM, CVLM, or VNS stimulation in rats. All three sites achieved high-precision control (Control Degree: RVLM 98.02%, CVLM 98.11%, VNS 98.49%) and minimal fluctuation. Non-invasive sonogenetics employed virus vectors to express mechanosensitive ion channel TRPC6. Significant tachycardia was evoked specifically at a pulse repetition frequency (PRF) of 800 Hz and high pressure (1.24 MPa, achieved with 600 mVpp input). No response occurred at lower pressure (0.63 MPa) or PRFs (20-400 Hz), or in control group expressing tdTomato, or in the non-injected hemisphere.

Electrical stimulation of the RVLM and CVLM provides precise, rapid, and effective bidirectional control of the heart rate with closed-loop method. The non-invasive sonogenetics approach opens novel pathways for clinical neuromodulation without implants. This work provides the foundation for next-generation neuromodulation therapy of cardiovascular diseases.

# Chapter 1 General introduction

The cardiovascular system plays a vital role in the circulating function which maintains daily somatic activity. To achieve a stable life support or provide catabolic metabolic organism for emergency conditions, the heart is innervated by two branches: the sympathetic nervous system and the parasympathetic nervous system. With opposite chronotropic and dromotropic effects, the two components regulate the heart by feedback loops of afferent and efferent innervations between the peripheral and central nervous systems.

**Cardiac autonomic innervation in the peripheral nervous systems**

The sympathetic trunks, leaving from the rostral ventrolateral medulla (RVLM), join bilaterally in the intermediolateral zone of the spinal cord including a dense part in the grey matter and extending part into the white matter. In the spinal cord segments T1-T5, sympathetic neurons contribute to the preganglionic cardiac part of the sympathetic chain with multiple postganglionic projections[1]. Although lacking a clear investigation, sympathetic neurons in discrete segments are arranged as specific cardiac functions. Dembowsky et al identified different types of preganglionic neurons with distinct electrophysiological characteristics in T3 segment of cats[2]. Transneuronal tracing showed that the preganglionic neurons in the upper thoracic segments projected to different regions to the heart of the dogs[3]. Paravertebral ganglia located bilaterally on the anterolateral side of the vertebral column are synapsed with preganglionic fibers at the same level, ascending or descending level in the sympathetic chain. Stellate, or cervicothoracic ganglion, consists of the inferior cervical ganglion and the first thoracic ganglion, provides the heart with postganglionic sympathetic axons[4–6]. Postganglionic nerves travel to the heart as separate nerves, rather than other destinations via gray rami with the spinal nerves[7]. Before reaching the heart, the cardiac nerves extend along the arteries including the common carotid, the subclavian and the brachiocephalic trunks. The cardiac nerves also run along the superior vena cava[4]. Fine postganglionic nerve trunks converge with cardiac vagus branches to form cardiac plexuses located at the aortic arch and the ascending aorta[8,9]. Postganglionic nerves originating from the bilateral stellate ganglions specifically innervate regions of the heart. Pardini et al observed the reduced noradrenalin level of the right ventricle after ganglionectomy of the left middle cervical-stellate ganglion[10]. Furthermore, several studies using electrical stimulation have shown that the left stellate ganglion shows a predominate inotropic effect, whereas the right stellate ganglion causes a significant chronotropic effect[11,12]. Such regional specificity can be extended to different segment levels and action potentials of the cardiac muscles[13]. The discrete innervation feature also results in different responses of heart rate and contractile force in

localized regions of the right and left ventricles by electrically stimulating different branches of cardiac postganglionic nerves[14–16].

The parasympathetic motor nerves are carried by the vagus nerve originating from the medulla[17]. The filaments of vagus nerve converge as one fiber at the jugular foramen and exit the brain stem. The vagus nerves bilaterally travel through the neck in the carotid sheaths between a common carotid and an internal jugular vein. Each carotid sheath is protected by three fascial layers. The vagus nerve bifurcates to form the recurrent laryngeal nerve and travels to the heart and cardiac plexuses. The left and right cervical vagus nerves also differ in the innervation of heart regions[18,19]. The right vagus nerve projects more fibers to the cardiac atria and sinoatrial node[20], greatly reduced heart rate during stimulation[21]. The left cervical vagus nerve innervates the atrioventricular node, showed no effect on heart rate even under high level stimulation[22,23] and has been recommended as a stimulation target to relieve cardiovascular side effects[20,24,25].

The sympathetic postganglionic nerve branches and preganglionic cardiac vagal branches converge to form cardiac plexuses and enter the heart together[26]. Both cardiac sympathetic and parasympathetic nerves densely innervate the sinoatrial node, atrioventricular nodes and conducting tissue[7,27]. Sympathetic nerves maintain the basal autonomic activity of the sinoatrial node and atrioventricular nodal conduction. The activity in vagal fibers to the heart causes inhibition of pacemaker cells and decreases excitability at the atrioventricular nodes[28].

**Medullary output control of the cardiac autonomic activity**

The ventrolateral medulla (VLM) in the lower brainstem extending rostrocaudally from the caudal pole of the facial nucleus to the spino-medullary junction is regarded as a key cardiovascular regulatory center[29,30]. The catecholaminergic neurons founded in the VLM are subdivided into adrenergic neurons rostrally (C1 cells) and noradrenergic neurons caudally (A1 cells)[31,32]. And the intermediary region between containing a mix of C1 and A1 clusters, which is extremely heterogeneous and harbors cardiovagal neurons and inhibitory GABAergic interneurons that mediate the sympathetic baroreflex[33]. The rostral portion of the VLM (RVLM) have been defined as the sympathoexcitory area extending with the C1 neurons. While the caudal VLM (CVLM) was typically identified via noradrenergic neurons (A1 group) or cardiovascular effect (vasodepressor area)[33,34]. In this research the CVLM is defined by its anatomical location, rostral to the caudal end of the RVLM with sympathoinhibitory function[34]. The RVLM sends excitatory projections to preganglionic sympathetic neurons located in the intermediolateral cell columns in the spinal cord. Other discreate regions within the brain stem and the hypothalamus also contribute to the central sympathetic output: the rostral ventromedial medulla, midline medulla,

the A5 noradrenergic cell group, and the paraventricular nucleus in the hypothalamus[35]. Whereas in bilateral inactivation or ablation experiments only the RVLM directly result in a significant vasodepressor and sympathoinhibitory effect[36]. These studies indicate that the discharge of RVLM neurons forms the background level of sympathetic nerve activity. The mechanisms that underlie such discharge assume that the presympathetic neurons have an intrinsic auto-depolarization property, and the tonic resting activity depends on synaptic inputs[33,36]. RVLM neurons mediate various somatic and visceral sympathetic reflexes via GABAergic inhibition from the brain stem areas including the caudal pressor area, midline depressor area, nucleus tractus solitarius and gigantocellular depressor area, which is then reflected through the fluctuation of sympathetic nerve activity and blood pressure[37–40]. Especially since the strong GABA-mediated input from CVLM containing barosensitive neurons with pulse-modulated activity and baroreceptor-independent neurons with tonic sympathoinhibition plays a critical role in the baroflex[41–43]. The background activity of presympathetic neurons to the cardiovascular system stems from the integration of autoactivating properties and the network of synaptic inputs[44–46].

Both the nucleus ambiguous (NA) and the dorsal motor nucleus of the vagus nerve (DMN) send general visceral efferent vagus nerves to the organ ganglia as preganglionic parasympathetic fibers[47]. The NA inhibits cardiac function via fast B-fibers which release acetylcholine at the sinoatrial and atrioventricular nodes in a beat-to-beat pattern[19,48]. The DMN innervates the cardiac ganglia via slower C-fibers and contributes to the heart rate atrioventricular conduction and contractility to a lesser magnitude[49,50]. The activity of cardioinhibitory neurons in NA is intrinsically silent and relies on synaptic input from other neurons[51]. The NA receives excitatory inputs from barosensitive neurons in the nucleus of the solitary tract via glutamate release and inhibition during inspiration by GABAergic neurons in the local spinal circuits and the medullary ventral respiratory group[28].

**The imbalance of cardiac activity and neuromodulation**

The heart essentially requires the balance between sympathetic and parasympathetic nervous activities to run nomarlly. The alteration of autonomic nervous activity has been shown to trigger and worsen cardiovascular diseases including cardiac arrhythmias and hypertension. As evidenced by the occurrence of synchronous activity of the sympathetic and vagus nerve before the onset of atrial fibrillation (AF)[52,53]. In ventricular arrhythmias (VA), increased sympathetic tone reduced cardiac electrophysiological stability and promoted the incidence of VA. Whereas parasympathetic stimulation results in the antiarrhythmic effect[54–58]. Long-term hypertension has

been found to be accompanied with elevated sympathetic nerve activity and blood pressure is regulated by RVLM barosensitive neurons[29,59–61].

Therefore, autonomic nervous system (ANS) modulation emerged as an effective and promising therapy via moderating sympathetic hyperactivity and vagal stimulation in the cardiovascular field. The carotid sinus nerve placed at the pole of the internal carotid artery with baroreceptors, is involved in main baroreflex. Carotid baroreceptor stimulation enhancing baroreflex and sympathoinhibition effects has been shown to be effective in the long-term reduction of blood pressure in resistant hypertension[62–65]. Pulmonary vein isolation has been widely used to prevent depolarizations from the pulmonary vein as a treatment for AF[66] and can be combined with renal sympathetic denervation[67,68] and ganglionated plexi ablation[69,70]. Moreover, renal denervation has been applied to resistant hypertension by regulating kidney natriuresis and the renin-angiotensin system[71–75]. Cervical vagus nerve stimulation has been developed for implantation therapy of bioelectronics medicine. In clinical trials the vagus nerve stimulation via an implanted device has shown potential applications in treatment of heart failure[76–80].

As discussed above, current neuromodulation mostly employs an invasive method. Therefore, the potential complications of surgery and implants limit the promotion of invasive neuromodulation[81–83]. In this research, sonogenetics will be used to attempt non-invasive neuromodulation. To achieve bidirectional cardiac modulation with excitatory and inhibitory effects, the RVLM, CVLM, and NA region in the lower brainstem were used as target stimulation sites. Additionally, the cervical vagus nerve was also employed to examine the potential for cardiac modulation. The primary purpose of this study was to explore the precise and non-invasive method for controlling cardiac function via the medulla. The heart rate was employed as the index of cardiac activity. Firstly a series of open-loop electrical stimulation was performed to confirm the heart rate response to different stimulation parameters. The closed-loop stimulation with negative feedback control was time-targeted evaluated for period cardiac modulation, and the effect of autonomic rebalance was determined via intraperitoneal injection of neostigmine and dobutamine. Finally, adeno-associated virus (AAV) vector was injected into the VLM region to express the mechanosensitive channel TRPC6 for ultrasound irradiation. This includes evaluating the cardiac modulating effects of ultrasound parameters: pulse repetition frequency (PRF), and intensity.

# Chapter 2 Open-loop cardiac neuromodulation by medulla stimulation

## 2.1 Abstract

To evaluate the cardiac modulation ability of the medulla and cervical vagus nerve, different stimulation parameters were used to elicit chronotropic effect. In medulla stimulation, the results showed that the stimulus frequency elicited string cardiac effects during a 10 s open-loop stimulation. In vagus nerve stimulation both the frequency and intensity of the stimulus can influence cardiovascular effects.

## 2.2 Materials and devices

| Item | Article No. | Source |
|---|---|---|
| Wistar male rats | Slc<br>Kwl | Shimizu Laboratory Supplies<br>Kiwa Laboratory Animals |
| Coaxial needle electrode | IMB-9004 | Inter Medical, Japan |
| Bipolar hook electrode | IMM2-5050 | Inter Medical, Japan |
| Dual-channel amplifier | MEG-5200MG | Miyuki Giken |
| Stimulus generator | STG-4002 | Multi Channel Systems |
| AD/DA converter | PowerLab 16/35 | AD Instruments, Australia |
| Physiological - Biological Temperature Controller | TMP-5b | Supertech Instruments |
| 4,6-Diamidino-2-phenylindole Dihydrochloride | 19178-91 | Nacalai tesque |
| Data acquisition software | LabChart Pro | AD Instruments, Australia |

## 2.3 Methods

**General operations**

Nine Wistar male rats were used in the experiments (300-500 g). All experiments were approved by the Animal Ethics and Administrative Council of Hokkaido University and Kindai University. The rat was initially anesthetized in an induction chamber with 4-5% isoflurane. Once the animal failed to elicit the toe pinch reflex, the rat was sustained with inhalation anesthesia of 1-2% isoflurane and mounted in a stereotaxic apparatus. The body temperature was maintained at 37℃ by a heating pad. The rat forelimbs were attached with Ag/AgCl electrodes for electrocardiogram (ECG) lead I. The ECG signals were filtered at 1.5 to 100 Hz and amplified, followed by digitization at 1 kHz through a PowerLab data acquisition device.

**Open-loop stimulation**

To figure out the main factor influencing chronotropic response, various frequencies and currents were applied to the electrical stimulation of the RVLM, the CVLM and the cervical vagus nerve. For the ventrolateral medulla stimulation, a small craniotomy was performed above the RVLM (from bregma: 12.36 mm posterior, 2.3 mm lateral) or CVLM (from bregma: 13.20 mm posterior, 2.2 mm lateral) on the right side. A coaxial needle electrode (0.4 mm diameter) was inserted at the site at a depth of 8.2 mm from the dura. The electrical stimulation was performed via a stimulus generator using the following parameters (60 and 100 Hz, 20, 45 and 60 μA, 0.5 ms pulse width, biphasic square pulses), and each stimulation configuration was repeated three times. In the cervical vagus nerve stimulation experiments, the rat was placed in the supine position. After the incision was made at 1 cm lateral to midline, the cervical vagus, jugular vein and common carotid were exposed by blunt dissection. Following gentle isolation of the right vagus nerve from the carotid sheath, a hook electrode (0.5 mm diameter, 5 mm spaced) was placed around the nerve and secured with drops of liquid paraffin. The anode cephalad to cathode vagus nerve stimulation (VNS) was biphasically delivered at 0.2 ms pulse width to evaluate combinations of frequency and intensity (20 and 30 Hz, 0.1, 0.2 and 0.4 mA) with three repetitions.

**Histology**

To verify the location of stimulation, the electrode was coated in DiD (D7757, Thermo Fisher Scientific) via dipping it in 1 mg/mL solution. After electrical stimulation experiments, each rat was euthanized with combination anesthetics (medetomidine 0.15 mg/kg, midazolam 2 mg/kg, butorphanol 2.5 mg/kg) and overdosed in isoflurane. Brains were harvested and post-fixed in 4% paraformaldehyde (PFA) for 3 days at 4 °C after transcardial perfusion with saline, followed by 4% PFA. Tissues then were gradient cryoprotected in 15% and 30% sucrose solution and embedded in optimal cutting temperature medium. Frozen tissues were sectioned at 50 μm (Leica CM3000 Cryostat). Slides were permeabilized in 0.1 mol/L phosphate-buffered saline (PBS) with

0.3% Triton X-100, and incubated with 1 μg/mL DAPI in phosphate buffer. Following washing, the coverslip was applied with antifade mounting medium (50% glycerol + 2.5% DABCO in PBS). The locations of stimulation sites were confirmed on a Zeiss LSM 900 confocal microscope.

**Data analysis**

For each combination of parameters, ECG signals were continually recorded and divided in 10 s pre-stimulation baseline, and 10 s of cardiac response during the period of stimulation, and post-stimulation. The offline analysis on LabChart software with ECG analysis module was used to detect waves, beats and calculate intervals. The peak-to-peak RR intervals were used to evaluate the overall chronotropic effect was calculated from the relative change between baseline and period of stimulation. The dromotropic effect was determined via the obtained beat-to-beat PR intervals. To evaluate the efficacy of stimulation, indices of heart rate variability (HRV) in the time domain are presented including standard deviation of RR intervals (SDRR), and the SD1 and SD2 of the Poincaré plot.

All data are presented as mean ± standard error of the mean. The statistical tests used are explained in the legend of each figure. $P < 0.05$ was considered as statistical significance in all cases. Statistical analyses were performed with OriginPro software.

## 2.4 Results

The evoked chronotropic response to medulla stimulation was dependent upon frequency and intensity, Figure 1 illustrates a representative response to electrical stimulation of the rostral and caudal catecholaminergic medulla region. Electrical stimulation was delivered at a 500 μs pulse width. Low intensity stimulation (25 μA) evoked almost no change in basal chronotropic function. Increasing the intensity to 40 μA resulted in tachycardia or bradycardia during the on-phase in the rostral or caudal medulla. Analogously, only high-frequency stimulation induced chronotropic response during the on-phase of stimulation.

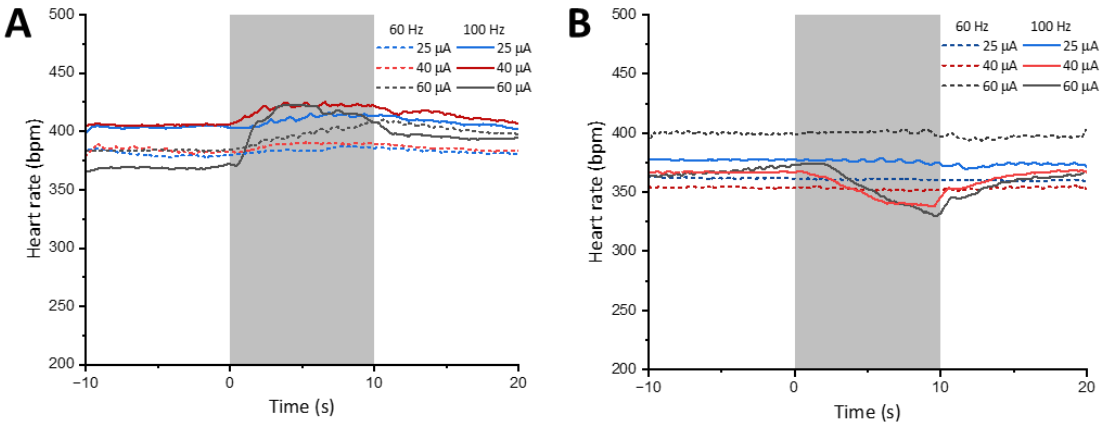


Figure 1. Typical heart rate trajectory during the electrical stimulation (grey area) in (A) RVLM and (B) CVLM.

Average chronotropic response (percentage change from baseline) in response to medulla stimulation are summarized in Figure 2. The chronotropic response during on-phase stimulation occurred preferentially at higher frequencies. High frequency afforded a greater range of control with increased sensitivity to chronotropic response to stepping changes in intensity.

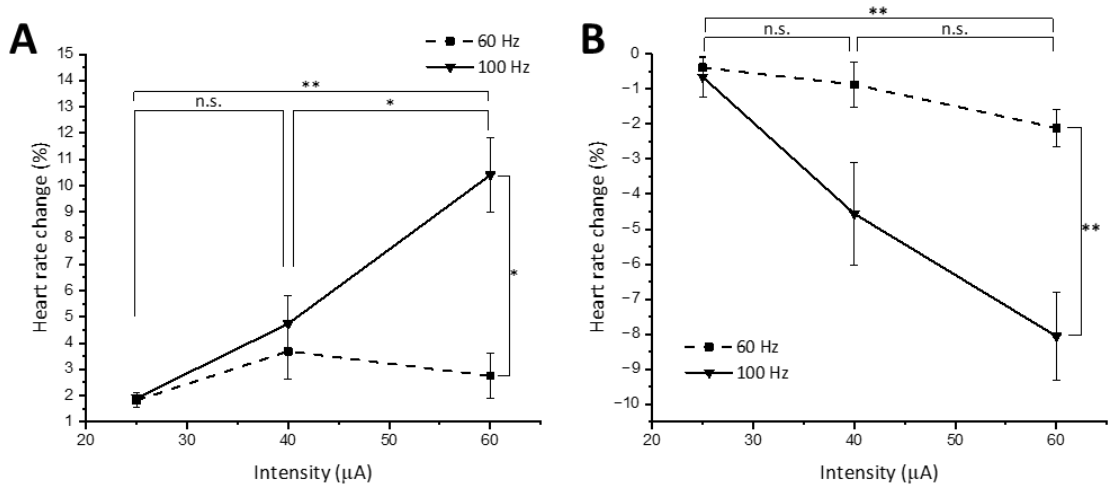


Figure 2. Mean heart rate change from baseline heart rate in electrical stimulation of (A) RVLM and (B) CVLM. *$p < 0.05$, **$p < 0.01$, n.s.: not significant by Fisher LSD multiple comparisons test following two-way ANOVA. Data are presented as mean ± SEM.

Additionally, the amplitude of heart rate changes was characterized by the standard deviation of RR interval (SDRR) as shown in Figure 3. At a high level of frequency, the chronotropic response evoked by stimulation resulted in a higher peak value, which represents a sustained heart rate change rather than a threshold-like patterned trajectory during the on-phase of stimulation. In rostral medulla stimulation using low frequency of 60 Hz with high intensity (60 μA), the increased SDRR shows a slight chronotropic effect which is indistinguishable in average percentage change (Fig. 3A).

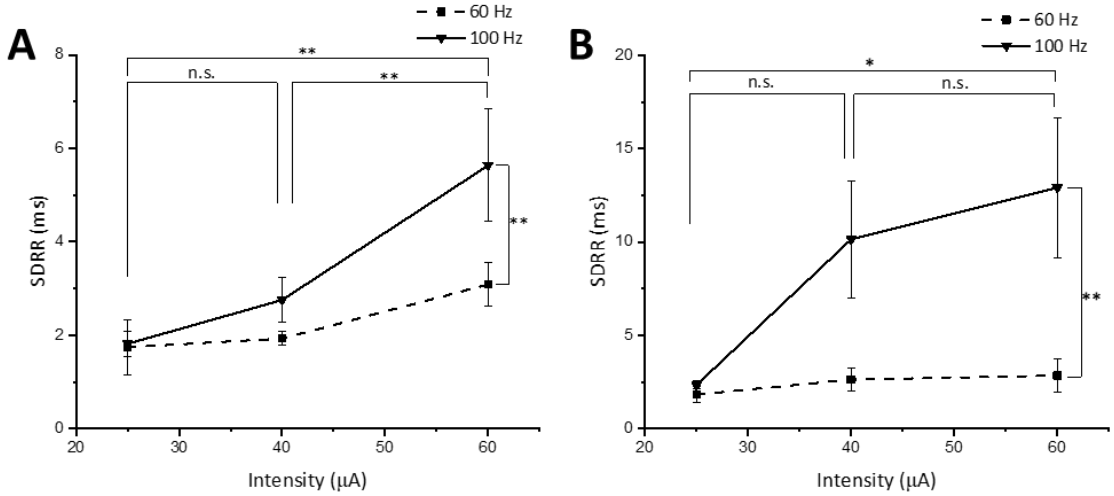


Figure 3. Standard deviation of RR interval during stimulation in (A) RVLM and (B) CVLM, which represents the amplitude of heart rate change. *$p < 0.05$, **$p < 0.01$, n.s.: not significant

by Fisher LSD multiple comparisons test following two-way ANOVA. Data are presented as mean ± SEM.

Figure 4 illustrates the change rate of chronotropic response during stimulation by SD1 and SD2 from the quantitative Poincaré plot. In SD1, which represents the variation of adjacent heartbeat, there was no significant difference at all combinations of parameters in both rostral and caudal medulla stimulations. For the long-term variation of SD2, there were analogous characteristics with SDRR where high frequency rapidly induced chronotropic response, and a slight response was demonstrated in the stimulation using 60 Hz and 60 μA.

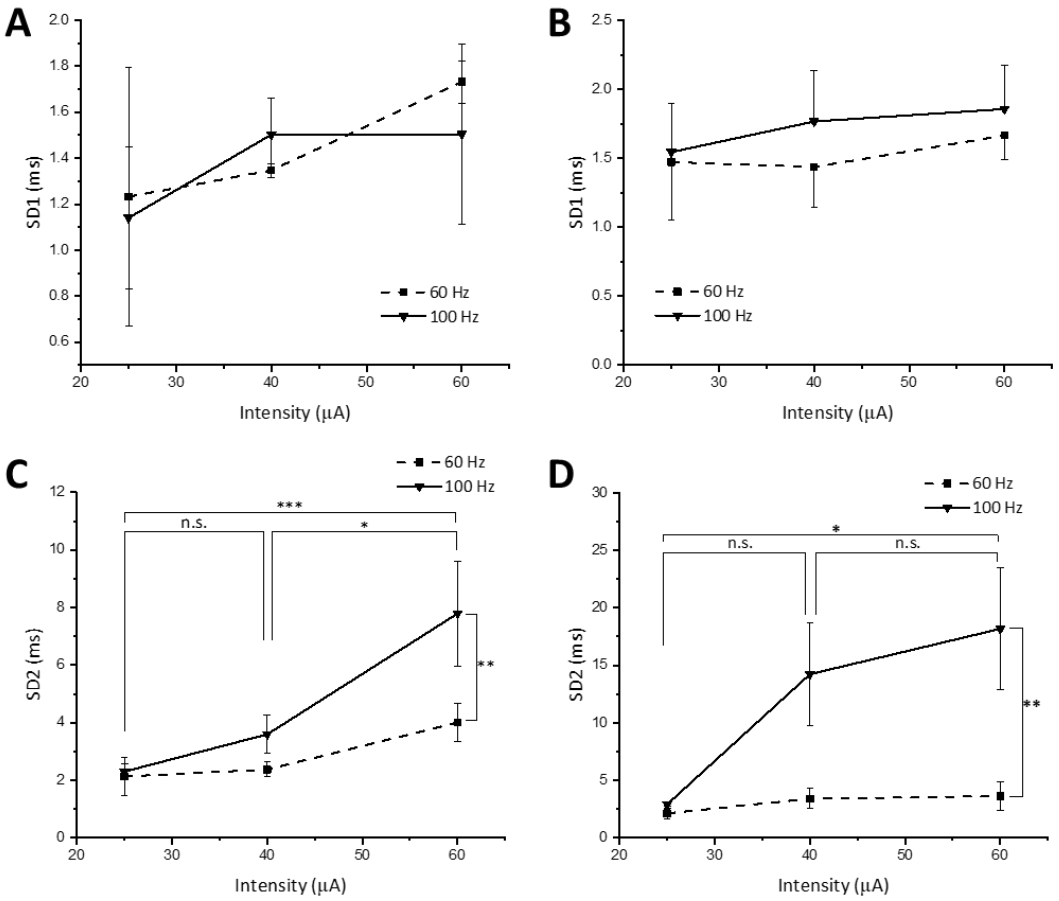


Figure 4. Quantitative SD1 and SD2 values from Poincaré plots during stimulation of (A), (C) RVLM and (B), (D) CVLM. *$p < 0.05$, **$p < 0.01$, ***$p < 0.001$, n.s.: not significant by Fisher LSD multiple comparisons test following two-way ANOVA. Data are presented as mean ± SEM.

The sympathetic nerve trunks innervate the local region of the ventricles. It should also be considered that medulla stimulation induces dromotropic effect. Figure 5 demonstrates the percentage change of PR interval from baseline. In the rostral medulla, the shortened conduction

time was enhanced by increased frequency and intensity. The stimulation of the caudal medulla evoked no change in dromotropic function at all levels of stimulation parameters.

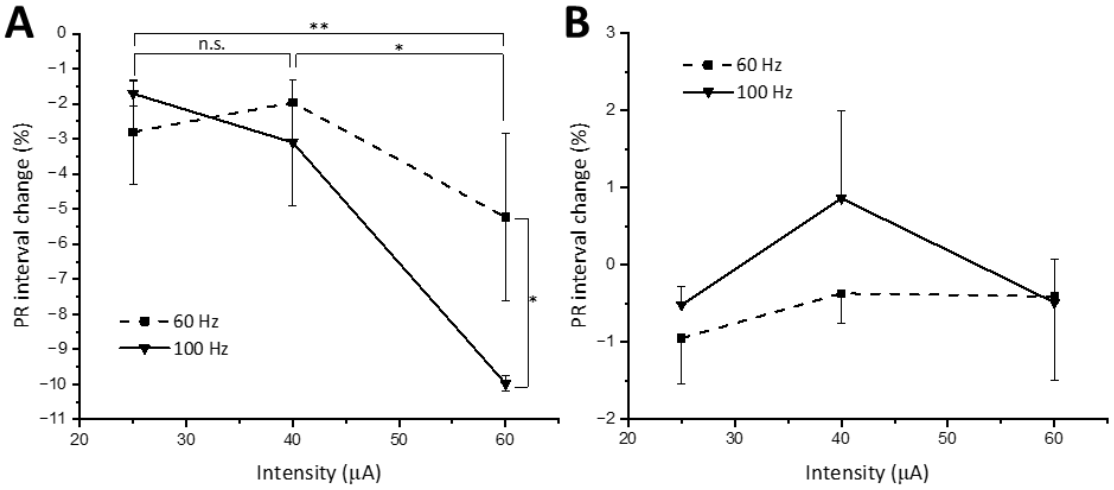


Figure 5. Percent changes of PR interval during electrical stimulation in (A) RVLM and (B) CVLM, which represents the changes of cardiac conductive function. *$p < 0.05$, **$p < 0.01$, n.s.: not significant by Fisher LSD multiple comparisons test following two-way ANOVA. Data are presented as mean ± SEM.

Vagus nerve stimulation evokes cardioinhibitory effect by enhancing parasympathetic nerve activity. To compare this function with caudal medulla stimulation, the right cervical vagus nerve of rats was stimulated at 20, 30 Hz and intensity of 0.1, 0.2, 0.4 mA. Figure 6 shows the cardiac effects of vagus nerve stimulation at the combinations of every parameter. While the chronotropic response is analogous to caudal medulla, the increasing intensity VNS evoked a more pronounced bradycardia effect at both 20 and 30 Hz (Fig. 6A). There was no significant difference between the two frequencies while the curves of average chronotropic responses show the tendency that the bradycardia to higher frequency of VNS was enhanced (Fig. 6B). The amplitude (Fig. 6C) and long-term variation (Fig. 6F) of heart rate change have the same characteristics, in which the effects were saturated at 0.4 mA. Figure 6E shows the same short-term variation at all levels of VNS. For dromotropic effects, the prolonged PR interval effects have a threshold of 0.2 mA while the conduction block was enhanced at the higher frequency.

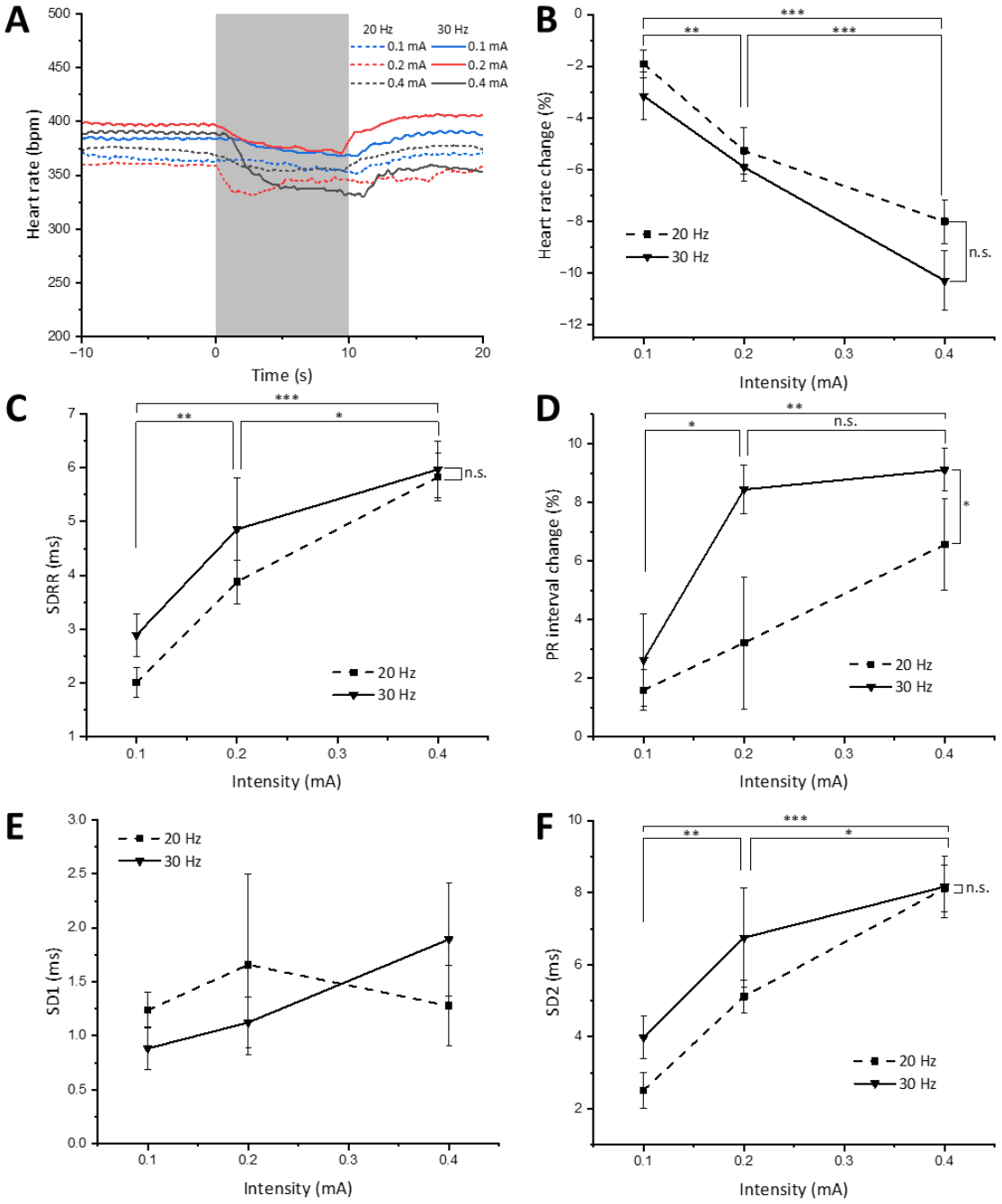


Figure 6. Cardia effects invoked by vagus nerve stimulation including (A) typical heart rate trajectory, (B) mean heart rate change, (C) standard deviation of RR interval, (D) percent change of PR interval, (E) and (F) quantitative values of Poincaré plots. *$p < 0.05$, **$p < 0.01$, ***$p < 0.001$, n.s.: not significant by Fisher LSD multiple comparisons test following two-way ANOVA. Data are presented as mean ± SEM.

## 2.5 Discussion

The RVLM region tonically excites sympathetic neurons and maintain the resting vasomotor tone. The adrenergic C1 neurons in RVLM innervate different segments of the intermediolateral column which impacts different cardiac functions via local postganglionic innervation. This study demonstrates that the cardiac responses depend on the stimulus frequency or intensity, suggesting that similar groups of neurons in the ventrolateral medulla provide the potential to control autonomic output based on specific physiological index. Moreover, the tonic sympathetic output can be finely modulated by variable stimulus frequency.

Autonomic control of regional cardiac function ultimately depends on the levels of sympathetic and parasympathetic activities and the interactions between them. Many cardiovascular diseases are associated with sympathetic hyperactivity which induces the remodeling of the cardiomyocyte and the cardiac plexuses that impacts cardiac electrical and mechanical functions. As demonstrated herein, the caudal medulla stimulation evoked the cardioinhibitory effects via inhibiting sympathetic output, which are different from muscarinic blockade effects elicited by VNS with conduction block. This finding suggests that caudal medulla stimulation can be deployed as an alternative neuromodulation therapy or a tool to explore cardiac remodeling during the progression of cardiovascular diseases.

# Chapter 3 Closed-loop control of heart rate by medulla stimulation

## 3.1 Abstract

In this study, the time-targeted cardiac modulation ability was evaluated on arbitrary static setpoints and drug administration. The setpoints were +20% and -10% of the baseline for positive and negative heart rate control respectively. The dobutamine or neostigmine was then intraperitoneally administrated to simulate the autonomic imbalance of diseases. Following the heart rate change elicited by administration of dobutamine and neostigmine, the stimulation was performed to reverse the deviation between the real-time and baseline heart rate. These closed-loop cardiac modulations were completed via closed-loop control.

## 3.2 Materials and devices

| Item | Article No. | Source |
|---|---|---|
| Wistar male rats | Slc<br>Kwl | Shimizu Laboratory Supplies<br>Kiwa Laboratory Animals |
| Coaxial needle electrode | IMB-9004 | Inter Medical, Japan |
| Bipolar hook electrode | IMM2-5050 | Inter Medical, Japan |
| Dual-channel amplifier | MEG-5200MG | Miyuki Giken |
| Stimulus generator | STG-4002 | Multi Channel Systems |
| AD/DA converter | PowerLab 16/35 | AD Instruments, Australia |
| Data acquisition software | LabChart Pro | AD Instruments, Australia |
| Multi-I/O Processor | RX8 | Tucker-Davis Technologies |
| Physiological - Biological Temperature Controller | TMP-5b | Supertech Instruments |
| Dobutamine | / | Sawai Pharmaceutical |
| Neostigmine | / | Kyowa Pharmaceutical Industry |
| 4,6-Diamidino-2-phenylindole Dihydrochloride | 19178-91 | Nacalai tesque |

## 3.3 Methods

### General operations

Fifteen Wistar male rats were used in the experiments (300-500 g). All experiments were approved by the Animal Ethics and Administrative Council of Hokkaido University and Kindai University. The rat was initially anesthetized in an induction chamber with 4-5% isoflurane. Once the animal failed to elicit the toe pinch reflex, the rat was sustained with inhalation anesthesia of 1-2% isoflurane and mounted in a stereotaxic apparatus. The body temperature was maintained at 37℃ by a heating pad. The rat forelimbs were attached with Ag/AgCl electrodes for electrocardiogram (ECG) lead I. The ECG signals were filtered at 1.5 to 100 Hz and amplified, followed by digitization at 1 kHz through a PowerLab data acquisition device.

### Closed-loop system

A multi-I/O real-time processor (RX8, Tucker-Davis Technologies) loading the custom controller routine detected R wave threshold for computing real-time heart rate and generated the trigger to a stimulus generator (STG-4002, Multi Channel Systems) by a bang-bang closed-loop law (Fig. 7).

From the previous results of open-loop stimulation, the high level stimulus frequency of 100 Hz can rapidly induce cardiac effects and saturate heart rate change. To investigate the maximum control ability of heart rate via medulla stimulation, the closed-loop stimulation with 100 Hz stimulus was set to sustain heart rate at desired values of +20% and -10% for tachycardia and bradycardia effect separately. Additionally, the animals were intraperitoneally injected with neostigmine (0.5 mg/kg) or dobutamine (0.4 mg/kg) to explore the control ability in the imbalanced autonomic environment with sympathetic or parasympathetic hyperactivity, respectively. After the heart rate was stably altered, the closed-loop stimulation was performed with the target value of the baseline heart rate. In these conditions, the appropriate stimulus frequency was calculated from the difference between altered heart rate and baseline heart rate to prevent saturation or oscillation in the control system caused by inter-individual variations of drug effect.

### Electrical stimulation

For the ventrolateral medulla stimulation, a small craniotomy was performed above the RVLM (from bregma: 12.36 mm posterior, 2.3 mm lateral) or CVLM (from bregma: 13.20 mm posterior, 2.2 mm lateral) on the right side. A coaxial needle electrode (0.4 mm diameter) was inserted at

the site at a depth of 8.2 mm from the dura. The electrical stimulation was performed via a stimulus generator using the following parameters (60 μA, 0.5 ms pulse width, biphasic square pulses). n the cervical vagus nerve stimulation experiments, the rat was placed in the supine position. After the incision was made at 1 cm lateral to midline, the cervical vagus, jugular vein and common carotid were exposed by blunt dissection. Following gentle isolation of the right vagus nerve from the carotid sheath, a hook electrode (0.5 mm diameter, 5 mm spaced) was placed around the nerve and secured with drops of liquid paraffin. The anode cephalad to cathode vagus nerve stimulation (VNS) was biphasically delivered at 0.2 ms pulse width to evaluate combinations of frequency and intensity (30 Hz, 0.2 mA). The basic sequence consisted of three periods: baseline, controlled period, post-stimulation.

**Data analysis**

Continuously acquired data from all channels in Labchart software were played back for cross-checking the online RR interval detection and the controlled stimulus. The efficacy of heart rate regulation was evaluated by a scalar variable, the control degree, computed the mean value of the proximity between the target and real-time heart rate trajectory as follows:

$$Control\ degree = \frac{\sqrt{\sum_{i=1}^{n}(HR_r - HR_t)^2}}{n \times HR_t} \quad (1)$$

where $HR_r$ is the real-time heart rate and $HR_t$ is the target heart rate. This value is presented as the percentage which 100% corresponds to heart rate was completely controlled at target value. The square root value avoids counteracting errors when oscillations occur around the target value. The standard deviation was calculated to evaluate the stability during the control period. To assess the speed of heart rate response, the time constant was obtained using the non-linear fitting function of the exponential function in OriginPro.

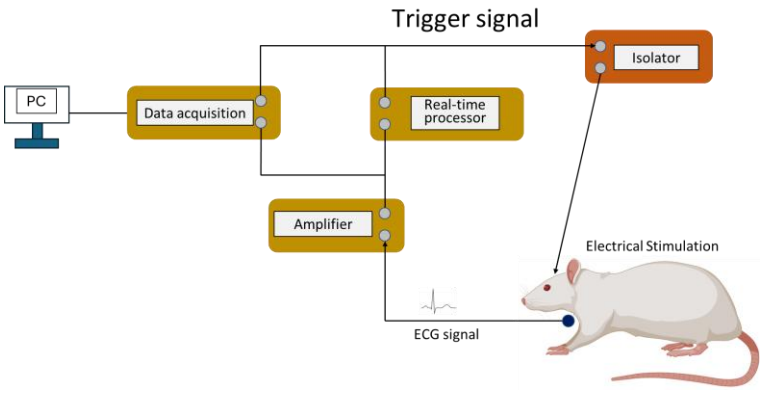


Figure 7. The schematic of the closed-loop stimulation system.

## 3.4 Results

To investigate the limit of control ability for precise heart rate regulation, I embedded the simple and robust control algorithms in the closed-loop medulla stimulation system. This on-off controller switched the stimulus when the heart rate trajectory crossed the target value. Figure 8 shows examples of the dynamic behaviors of controlled heart rate for the RVLM, CVLM and VNS. Note that the target value was set by the peak value of heart rate in open-loop stimulation.

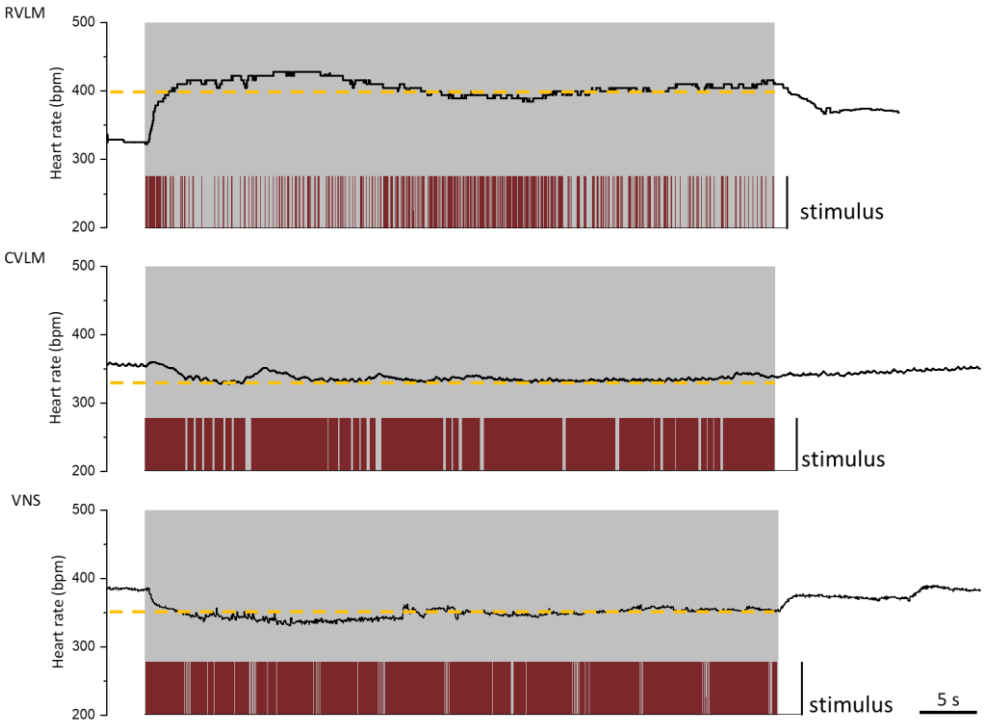


Figure 8. Examples of heart rate control in about 1 min (grey area) at target value of 120% and 90% from baseline (yellow dashed line) via electrical stimulation in RVLM, CVLM and VNS.

The control performance was quantified in terms of control degree, standard deviation and time constant (Fig. 9). In every experiment, the performance evaluation of control period was performed in offline analysis. The control degree of RVLM, CVLM and VNS were 98.02%, 98.11%, 98.49%, respectively. I observed that, compared to the VNS, the heart rate induced by closed-loop medulla stimulation had higher fluctuations corresponding to standard deviation, although the values of these standard deviations can be negligible due to the high resting sinus rhythm of rats. Overall, these results demonstrate that precise heart rate control can stably be conducted in closed-loop medulla stimulation. This medulla cardiac modulation could track the target value more rapidly compared to VNS (Fig. 9C).

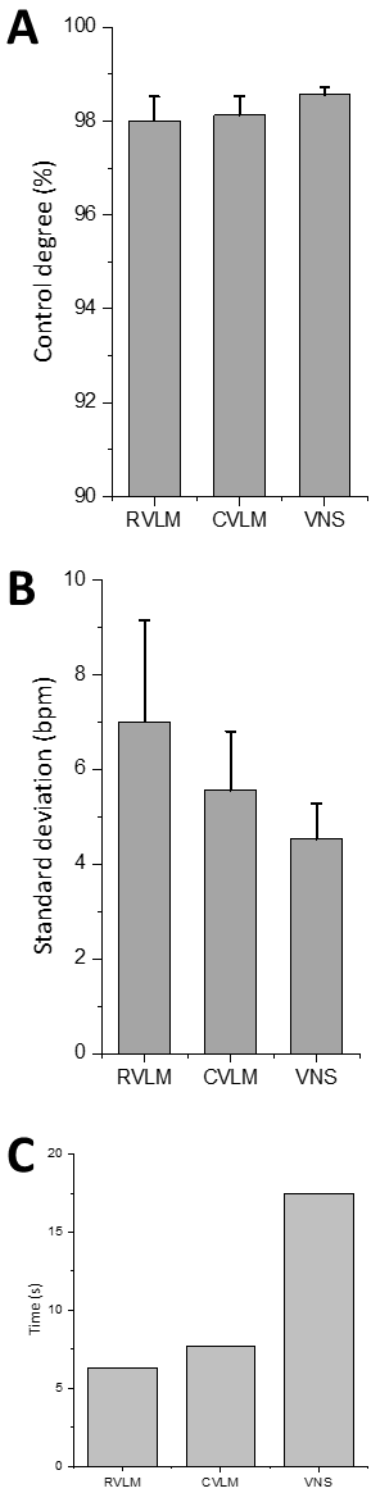


Figure 9. Evaluations of control effect including (A) control degree, (B) standard deviation and (C) time constant.

To investigate if the medulla stimulation can still exert the ability to regulate heart rate, the animals were intraperitoneally injected with the acetylcholinesterase inhibitor neostigmine or β1 receptor agonist dobutamine to simulate an imbalance of autonomic tone. Figure 10 shows a representative heart rate trajectory obtained in two experiments for reducing drug effects on heart rate. Note that the stimulus frequency was set by the level of sustained chronotropic drug effect from 60 to 100 Hz.

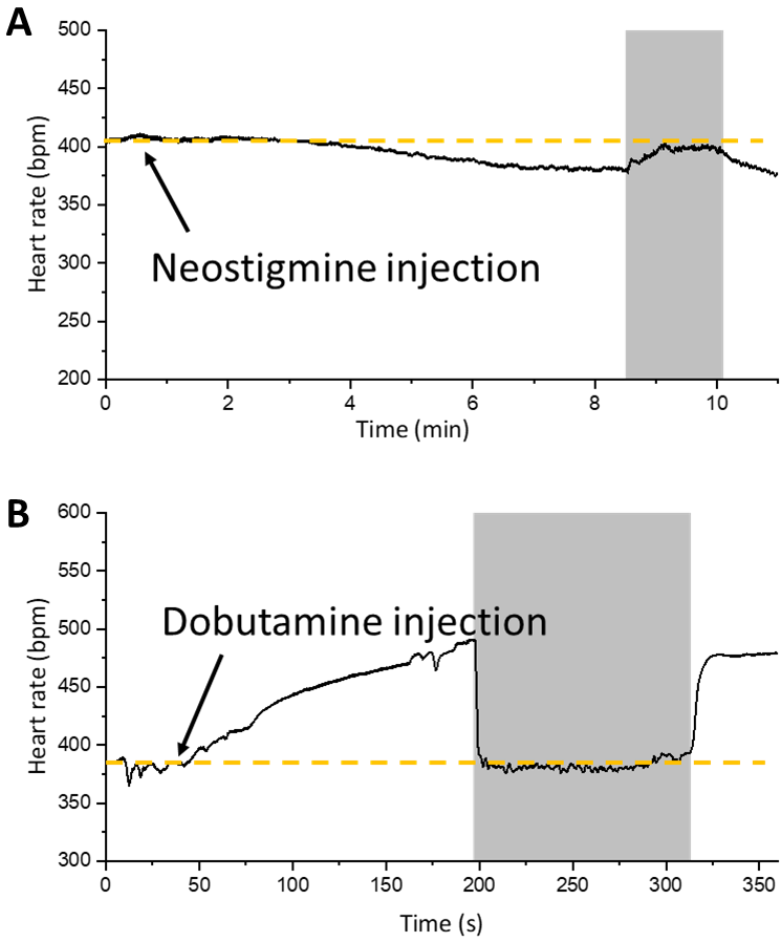


Figure 10. Examples of restoring heart rate to baseline (yellow dashed line) in autonomic imbalance caused by (A) neostigmine and (B) dobutamine injection. During electrical stimulation (grey area), the target values were set as baseline heart rate.

As shown in figure 11, the heart rate regulation induced by closed-loop medulla stimulation in drug-administrated rats could track the target value of baseline heart rate with slight fluctuation. The results in administrated rats were similar to those observed in normal rats. This demonstrates that the electrical stimulation of the medulla is still effective even during imbalanced autonomic activity and can temporarily normalize heart rate to its natural state.

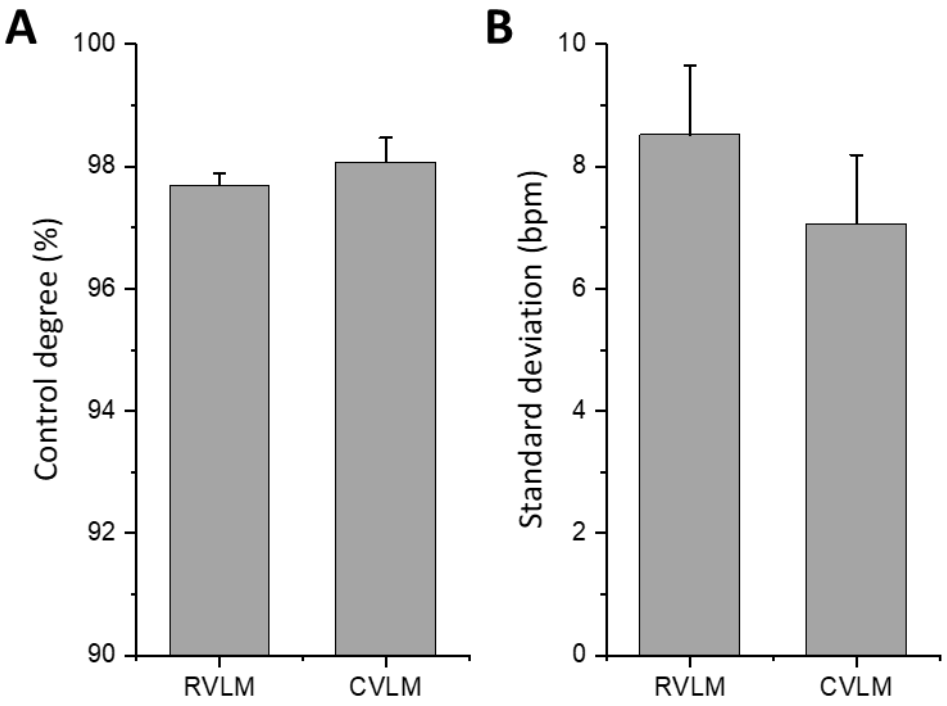


Figure 11. Evaluations of restoration experiments including (A) control degree and (B) standard deviation.

## 3.5 Discussion

Chronic tachycardia and hypertension caused by sympathetic hyperactivity lead to pathophysiological consequences. In animals and patients with hypertension myocardial and left ventricular remodeling are associated with elevated sympathetic outflow[84–86]. Accordingly, cardiac remodeling develops cardiac arrhythmias and increases the risk of sudden cardiac death[87]. Traditional pharmacological treatments are known to have hard-to-avoid side effects due to complex and sustained pharmacokinetic processes. With the anti-tachycardic effect, VNS has the potential as an alternative therapy to provide cardioprotective effects for drug-resistant patients. Appropriate bradycardia is necessary to prevent hypoperfusion and hold physical activities. The vagus nerve has a mixed fiber population that is classified as A-, B-, and C-fibers in accordance with diameter, myelination and activation thresholds. Due to the complex fascicular organization and function of the fibers, the stimulation effect depends on various factors such as frequency, current intensity, pulse width and electrode interface. Previous studies demonstrated many methods for accurate heart rate regulation including optimizing parameters by closed-loop control, cardiac-synchronized stimulation and electrode design[88–93]. In this study, the results show similar performance of heart rate control in the case of medulla stimulation with a simple on-off control strategy. To tonically active neurons in the medulla, the efficacy of control can be improved by optimizing the stimulus to match the desired set heart rate. The methodology of heart rate regulation in medulla stimulation will be easier and more predictable than traditional VNS and pharmaceutical treatments. Additionally, positive and negative modulation of sympathetic activity in the medulla to more scenarios can be envisioned.

# Chapter 4 Development of non-invasive cardiac neuromodulation in medulla using sonogenetics

## 4.1 Abstract

To effectively activate the neurons in medulla, the adeno-associated virus (AAV) vector was microinjected to express mechanosensitive ion channels to enhance ultrasound sensitivity. The pulse repetition frequency was varied and tachycardia was evoked at specific pulse repetition frequency and high ultrasound pressure.

## 4.2 Materials and devices

| Item | Article No. | Source |
|---|---|---|
| Wistar male rats | Slc<br>Kwl | Shimizu Laboratory Supplies<br>Kiwa Laboratory Animals |
| Piezoelectric ceramic | 1Z10DS15R-SYX | Fuji Ceramics |
| Function/arbitrary waveform generator | DG953 | Rigol |
| RF amplifier | T145-4726AA | Thamway |
| Dual channel amplifier | MEG-5200MG | Miyuki Giken |
| Stimulus generator | STG-4002 | Multi Channel Systems |
| AD/DA converter | PowerLab 16/35 | AD Instruments, Australia |
| Data acquisition software | LabChart Pro | AD Instruments, Australia |
| Physiological - Biological Temperature Controller | TMP-5b | Supertech Instruments |
| HA Tag Antibody | NB600-362 | Novus biologicals |
| Alexa Fluor® 488 AffiniPure® Donkey Anti-Goat IgG (H+L) | AB_2340428 | Jackson ImmunoResearch |
| 4,6-Diamidino-2-phenylindole Dihydrochloride | 19178-91 | Nacalai tesque |

## 4.3 Methods

### General operations

Seven Wistar male rats were used in the experiments (300-500 g). All experiments were approved by the Animal Ethics and Administrative Council of Hokkaido University and Kindai University. The rat was initially anesthetized in an induction chamber with 4-5% isoflurane. Once the animal failed to elicit the toe pinch reflex, the rat was sustained with inhalation anesthesia of 1-2% isoflurane and mounted in a stereotaxic apparatus. The body temperature was maintained at 37℃ by a heating pad. The rat forelimbs were attached with Ag/AgCl electrodes for electrocardiogram (ECG) lead I. The ECG signals were filtered at 1.5 to 100 Hz and amplified, followed by digitization at 1 kHz through a PowerLab data acquisition device.

### AAV injection

The genetic engineering experiments were approved by the institutional Recombinant DNA Experiment Committee. The recombinant adeno-associated viral vector AAVDJ-hSyn-TRPC6-HA, used for expressing mechanosensitive ion channel TRPC6, was provided by Dr. Masafumi Shimojo[94] (Advanced Neuroimaging Center, National Institutes for Quantum Science and Technology, Japan). For the sham group, AAVDJ-hSyn-tdTomato (Addgene#193019) was injected. Adult rats were anesthetized with 1-2% isoflurane for AAV injections. To target sympathetic neurons in the ventrolateral medulla, 300 nl AAV vector to each site was injected into wild type rats at the following stereotactic coordinates: 3.36 mm caudal to lambda, 2.1/2.3 mm lateral to lambda, 8.1/8.3 mm ventral to the brain surface. Rats recovered for at least 4 weeks before ultrasound irradiation experiments.

### Ultrasound irradiation

The pulses were generated using a function generator (DG953, Rigol) and amplified by a radio frequency amplifier (T145-4726AA, Thamway) before being sent to drive a bowl piezoelectric ceramic transducer (1Z10DS15R-SYX, Fuji Ceramics) with a 10 mm diameter, 15 mm focus length, and a center frequency of 1 MHz. The acoustic field distribution was measured using a calibrated needle hydrophone (NH0500, Eastek) in a water tank, and the transducer was attached to a 3D orientation frame. The full-width-at-half-maximum (FWHM) of the acoustic field was about 3.6 mm in the focal plane (Fig. 12B). To obtain acoustic pressure, the output signal of the function generator was adjusted from 50 to 600 mVpp. In this study, the ultrasound parameters were investigated to evoke cardiac effect are as follows: pulse repetition frequencies (PRF) = 20 / 40 / 80 / 200 / 400 / 800 Hz, output signal of function generator = 300 / 600 mVpp, fundamental

frequency = 1 MHz, duty cycle = 50%. The ultrasound transducer was mounted on the stereotaxic apparatus with a 3D-printed holder. The collimator was placed on the surface of the skull above the target brain region. Transcranial pulsed ultrasound was delivered to the RVLM (from bregma: 12.36 mm posterior, 2.3 mm lateral) with coupling ultrasound gel.

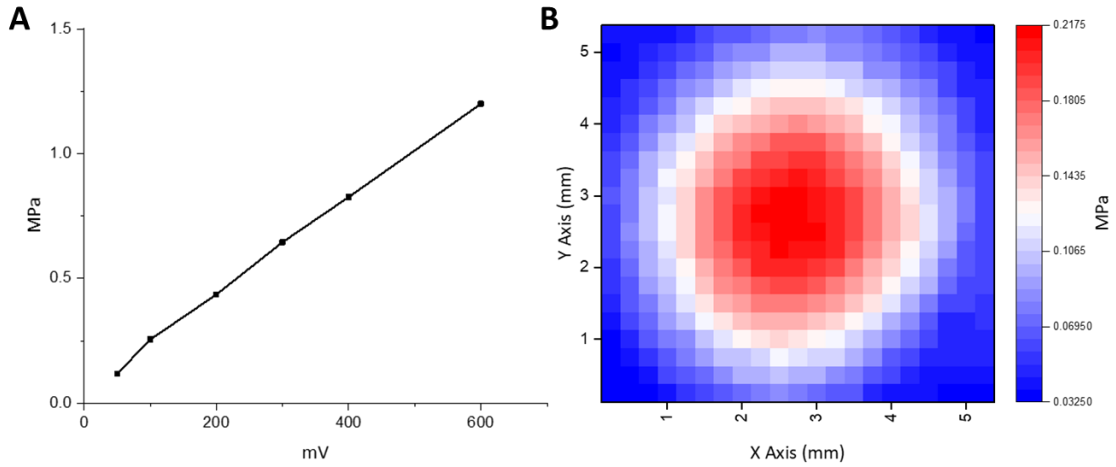


Figure 12. Ultrasound properties of the transducer. (A) Ultrasound pressure at the focal area corresponding to the output signal of the function generator. (B) The distribution of the ultrasound field at the x-y plane at 100 mVpp of function generator output.

**Histology**

After ultrasound stimulation experiments, each rat was euthanized with combination anesthetics (medetomidine 0.15 mg/kg, midazolam 2 mg/kg, butorphanol 2.5 mg/kg) and overdosed in isoflurane. Brains were harvested and post-fixed in 4% paraformaldehyde (PFA) for 3 days at 4 °C after transcardial perfusion with saline followed by 4% PFA. Tissues were then gradient cryoprotected in 15% and 30% sucrose solution and embedded in optimal cutting temperature medium. Frozen tissues were sectioned at 50 μm (Leica CM3000 Cryostat). Sections were blocked for 30 min in phosphate-buffered saline (PBS) with 0.3% Triton X-100 and 10% normal donkey serum, then incubated with primary antibody (Goat anti-HA, Novus biologicals, NB600-362, 1:1000) in block buffer (PBS + 0.3% Triton X-100 + 1% normal donkey serum) overnight. Slices were washed and incubated in secondary antibody (Donkey anti-goat IgG conjugated to Alexa Fluor 488, Jackson immunoresearch, AB_2340428, 1:1000) in block buffer for 2 h at room temperature. After washing with PBS, the sections were stained with 4',6-diamidino-2-phenylindole (DAPI) (19178-91, Nacalai tesque, 1 μg/ml). Following washing, the coverslip was applied with antifade mounting medium (50% glycerol + 2.5% DABCO in PBS). Stained neurons were imaged on a Zeiss LSM 900 confocal microscope.

## 4.4 Results

As a first step toward non-invasive cardiac neuromodulation, each animal was subjected to pulsed ultrasound (1 MHz frequency, 30 s duration, 20 to 800 Hz PRF at 50% duty cycle) with 600 mVpp output signal of the function generator which corresponds to a pressure of 1.24 MPa. The heart rate change was recorded including 30 s of stimulation duration. As shown in Fig. 3A, typical tachycardia was evoked specifically at 800 Hz PRF. And at 300 mVpp of output signal which corresponds to about 0.63 MPa, there was no cardiac response during the 30 s stimulation (n = 4, data not shown). The maximum heart rate change from the baseline was distinguishable from the other PRFs and the control group of tdTomato expression (Fig. 3B, $p < 0.001$, t-test). Note that the calculation between the maximum and baseline heart rate did not exclude the fluctuation of sinus rhythm in all conditions. I also tested the effect of PRF around 800 Hz and the same RVLM region in the other hemisphere, which did not receive microinjection of AAVs (Fig. 13C), holding all other parameters (i.e., pressure, duty cycle). The heart rate did not increase substantially except for 800 Hz PRF with virus injection, reinforcing the idea that the cardiac response depends on the expression of mechanosensitive ion channels and ultrasound stimulation at specific PRF.

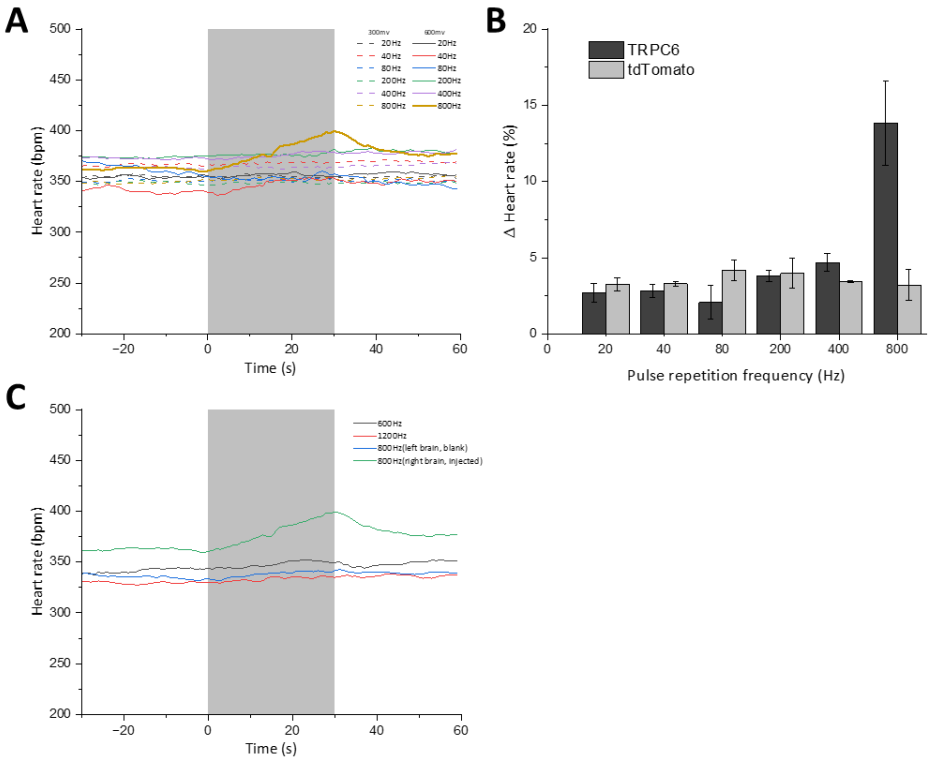


Figure 13. Ultrasound stimulation (grey area) evoked tachycardia at 800 PRF and 600 mVpp. (A) Typical heart rate trajectory in ultrasound stimulation. (B) Percent change of maximum heart rate

during stimulation and baseline heart rate in TRPC6 group and control group. (C) Ultrasound stimulation at PRF around 800 Hz and on the hemisphere without injection did not evoke cardiac effect.

I explored the expression of mechanosensitive ion channel in the RVLM region after ultrasound stimulation. As shown in Fig. 14A, HA-positive neurons were found in the RVLM region, while the lateral rostral ventromedial medulla (RVMM) region which also has vasomotor effect[34] did not express TRPC6 channel. To assess the biological safety of the ultrasound irradiation, DAPI staining was used to evaluate cell apoptosis. The labeled cells with intact reticular formation show no obvious cell damage in the target regions (Fig. 14B).

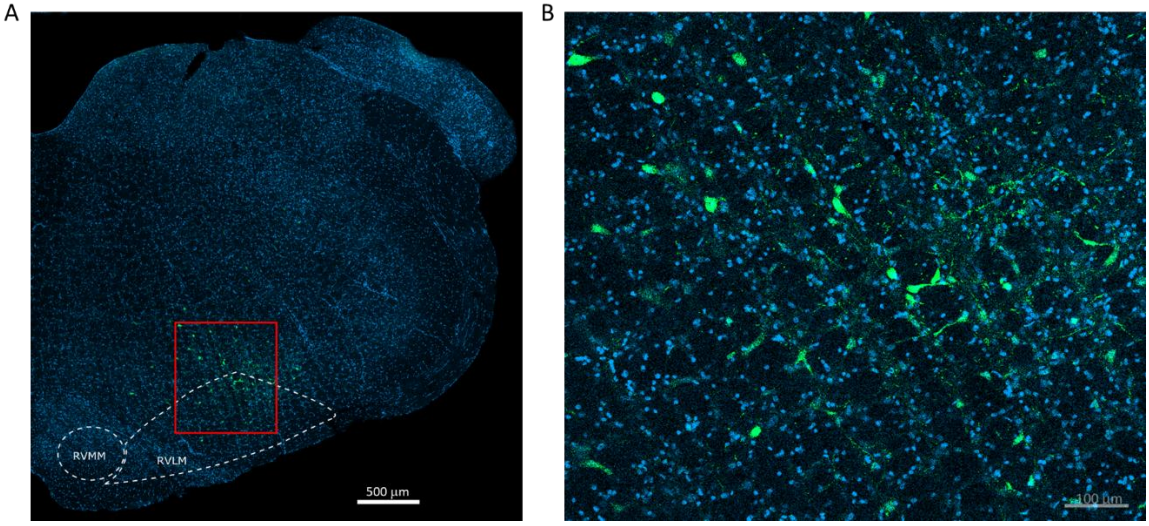


Figure 14. Spatial distribution of neurons expressing TRPC6 after AAV vector injection. DAPI is in blue and TRPC6 expressed neurons are in green as HA-tag of immunostaining.

## 4.5 Discussion

The mechanism underlying ultrasound stimulation evoking neural activity is still ambiguous at present. Two main effects have been considered during acoustic waves through tissues: thermal and mechanical domains. Ultrasound induces an increase in temperature that is capable of activating neurons whose membranes contain thermoresponsive ion channels, or increase blood flow and vascular permeability. Mechanical effects are physical effects including acoustic radiation force, acoustic streaming and cavitation. Acoustic radiation force arises from ultrasound absorption, scattering, reflection, standing waves or other phenomena. These propagations of acoustic waves result in the distribution of acoustic intensities, and lead to a steady pressure during ultrasound application on the target. Acoustic streaming induces steady oscillations with period equal to the fundamental frequency, and causes appreciable displacement of the cell membrane. Ultrasound may elicit cavitation, which entails the formation and collapse of gaseous cavities. The strong dependence of the stimulation effects on PRF that argues against a thermal explanation is nearly fatal for the hypotheses of cavitation and acoustic streaming as well. Because cavitation requires pressures larger than 5 MPa[95], the low pressure I used during these experiments makes cavitation unlikely. The brain tissue has a speed of sound at about 1515 m/s, the 1 MHz ultrasound deforms the cell membrane in a sinusoidal fashion along the wave length of ~1515 μm. It is questionable whether such a huge deformation can activate a small TRPC6 ion channel. Acoustic radiation force only creates movement during the on-phase of the ultrasound, and results in no effect during the off-phase in a cycle. Thus, these findings implicate acoustic radiation force as a major physical effect of ultrasound on neurons that expressed mechanosensitive ion channels. While such spiked responses are inconsistent with previous studies that showed the gradual curve between response and ultrasound PRF[96,97]. Iversen et al. also found that different types of neurons showd preferential response to the patterns of amplitude-modulated ultrasound[98]. Based on the results of previous chapters, it is necessary to establish the relationship between parameters and cardiac effect for precise heart rate regulation. Therefore, future work will be dedicated to varying PRF in small range around 800 Hz and modulate waveforms for controlling cardiac effect.

# Chapter 5 General discussion

**Sympathetic neuromodulation in medulla**

Dysfunction of autonomic nervous system plays a crucial role in the development and progression of many diseases. Therefore, modulating autonomic nervous system activity would be able to act on the internal state of the body and compensate for dysfunctional nervous circuits leading to disease. For decades, several devices have been developed as bioelectronic medicines for using electrical pulses to communicate with the nervous system to improve health as neural prostheses[99]. These devices mostly act on baroreflex and vagus nerve, which lack the scenario of sympathetic neuromodulation. Novel neural engineering was developed to miniaturize electrical devices, decipher and modulate neural signal patterns which are deployed as closed-loop strategies for the detection of dysfunctional activity and achieve therapeutic effects[100]. Although VLM neurons receive inputs to regulate sympathetic output from other central regions including the paraventricular nucleus of the hypothalamus, nucleus of the solitary tract, lateral tegmental field and A5 region. In this study, closed-loop control of the medulla can successfully intervene with tonic sympathetic output and alter the heart rate at the target value, which depends on adjusting stimulus frequency. This approach was also effective in the autonomic imbalance conditions caused by drug injections, which implicate the endogenous feedback regulation of sympathetic output may be limited and insufficient, and demonstrate potential therapeutic effects of medulla neuromodulation.

**Non-invasive neuromodulation toward controlling sympathetic hyperactivity**

Sustained change of cardiovascular homeostasis is associated with both changes in hormones and sympathetic nervous system. Brooks and Osborn have suggested a model stating that the raised sympathetic nerve activity is induced by an increased level of circulating angiotensin II[101], which can directly modulate blood pressure via activation of angiotensin II type 1 receptor thus causing vasoconstriction. The increase in blood pressure activates the baroreflex which leads to the inhibition of sympathetic efferents and decrease of blood pressure. However, this reflex in the nucleus of the solitary tract (NTS) can be reset to allow higher levels of blood pressure via the angiotensin II mediated pathway[102]. The mechanism of central sympathetic activity evoked via circulating angiotensin II has not been defined, probably involving the circumventricular organs which lack a blood-brain barrier and are rich in angiotensin II type 1 receptors. The RVLM neurons regulate renal sympathetic nerve[103,104], which facilitates renin release from the juxtaglomerular apparatus. It can be assumed that elevated sympathetic activity and angiotensin II level promote each other and are crucial to development of hypertension, together with a

baroreflex resetting in the NTS. Deep brain stimulation for sympathetic withdrawal has been shown to effectively reduce blood pressure in refractory hypertension[105,106] and centrally reset the blood pressure reflex[107]. Ultrasound stimulation offers the advantages of non-invasive and free from side effects for central neuromodulation. Previous studies demonstrated depressor effect using focused ultrasound[108,109]. In this work, the RVLM neurons were successfully activated to induce cardioexcitatory effects using sonogenetics. The limitations of applying ultrasound to depressor CVLM in experiments are the extent and caudal position close to the skull, which hardly complete specific stimulation and bring coordinate problem. Therefore, for future work, specific activation of the parasympathetic neurons in the medulla using selective AAV vector is planned.

# Acknowledgement

I would like to thank my advisors, Dr. Yuichi Takeuchi and Dr. Masabumi Minami of Hokkaido University and for providing guidance and support throughout this project. Without their guidance and persistent help this thesis would not have been possible.

I would like to thank Dr. Nobuki Kudo of Hokkaido University, who provided technical support of ultrasound experiments and introduced the concept of ultrasound engineering to me.

I would like to thank Dr. Masafumi Shimojo and Dr. Yumi Matsushita of National Institutes for Quantum Science and Technology, who provided necessary virus vectors for applying sonogenetics.

In addition, thanks to all members of laboratory of Pharmacology of Hokkaido University, and laboratory of pharmacotherapy of Kindai University. who offered me help and convenience in this project.

Reference


1. Bonica, J. J. Autonomic Innervation of the Viscera in Relation to Nerve Block. *Anesthesiology* **29**, 793–813 (1968).
2. Dembowsky, K., Czachurski, J. & Seller, H. Three types of sympathetic preganglionic neurones with different electrophysiological properties are identified by intracellular recordings in the cat. *Pflugers Arch.* **406**, 112–120 (1986).
3. Hopkins, D. A. & Armour, J. A. Localization of sympathetic postganglionic and parasympathetic preganglionic neurons which innervate different regions of the dog heart. *J of Comparative Neurology* **229**, 186–198 (1984).
4. Kawashima, T. The autonomic nervous system of the human heart with special reference to its origin, course, and peripheral distribution. *Anat Embryol* **209**, 425–438 (2005).
5. Zhang, B. *et al.* Anatomical variations of the upper thoracic sympathetic chain. *Clinical Anatomy* **22**, 595–600 (2009).
6. Pather, N., Partab, P., Singh, B. & Satyapal, K. S. Cervico-thoracic ganglion: Its clinical implications. *Clin. Anat.* **19**, 323–326 (2006).
7. Wink, J. *et al.* Human adult cardiac autonomic innervation: Controversies in anatomical knowledge and relevance for cardiac neuromodulation. *Autonomic Neuroscience* **227**, 102674 (2020).
8. Pather, N., Partab, P., Singh, B. & Satyapal, K. S. The sympathetic contributions to the cardiac plexus. *Surgical and Radiologic Anatomy* **25**, 210–215 (2003).
9. Kawashima, T. & Sasaki, H. Morphological comparison of the cardiac autonomic nervous system between normal and abnormal great arterial branching pattern with a brief review of the literature. *Autonomic Neuroscience* **132**, 37–43 (2007).
10. Pardini, B. J., Lund, D. D. & Schmid, P. G. Organization of the sympathetic postganglionic innervation of the rat heart. *Journal of the Autonomic Nervous System* **28**, 193–201 (1989).

11. Randall, W. C., Szentivanyi, M., Pace, J. B., Wechsler, J. S. & Kaye, M. P. Patterns of Sympathetic Nerve Projections onto the Canine Heart. *Circulation Research* **22**, 315–323 (1968).

12. Furnival, C. M., Linden, R. J. & Snow, H. M. Chronotropic and inotropic effects on the dog heart of stimulating the efferent cardiac sympathetic nerves. *The Journal of Physiology* **230**, 137–153 (1973).

13. Winter, J., Tanko, A. S., Brack, K. E., Coote, J. H. & Ng, G. A. Differential cardiac responses to unilateral sympathetic nerve stimulation in the isolated innervated rabbit heart. *Autonomic Neuroscience* **166**, 4–14 (2012).

14. Szentivanyi, M., Pace, J. B., Wechsler, J. S. & Randall, W. C. Localized Myocardial Responses to Stimulation of Cardiac Sympathetic Nerves. *Circulation Research* **21**, 691–702 (1967).

15. Ng, G. A. *et al.* Sympathetic nerve stimulation produces spatial heterogeneities of action potential restitution. *Heart Rhythm* **6**, 696–706 (2009).

16. Norris, J., Foreman, R. & Wurster, R. Responses of the canine heart to stimulation of the first five ventral thoracic roots. *American Journal of Physiology-Legacy Content* **227**, 9–12 (1974).

17. Câmara, R. & Griessenauer, C. J. Anatomy of the Vagus Nerve. in *Nerves and Nerve Injuries* 385–397 (Elsevier, 2015). doi:10.1016/B978-0-12-410390-0.00028-7.

18. Berthoud, H.-R. & Neuhuber, W. L. Functional and chemical anatomy of the afferent vagal system. *Autonomic Neuroscience* **85**, 1–17 (2000).

19. Ruffoli, R. *et al.* The chemical neuroanatomy of vagus nerve stimulation. *Journal of Chemical Neuroanatomy* **42**, 288–296 (2011).

20. Groves, D. A. & Brown, V. J. Vagal nerve stimulation: a review of its applications and potential mechanisms that mediate its clinical effects. *Neuroscience & Biobehavioral Reviews* **29**, 493–500 (2005).

21. Randall, W. C. & Ardell, J. L. Selective parasympathectomy of automatic and conductile tissues of the canine heart. *American Journal of Physiology-Heart and Circulatory Physiology* **248**, H61–H68 (1985).

22. Woodbury, D. M. & Woodbury, J. W. Effects of Vagal Stimulation on Experimentally Induced Seizures in Rats. *Epilepsia* **31**, (1990).

23. Stauss, H. M. Differential hemodynamic and respiratory responses to right and left cervical vagal nerve stimulation in rats. *Physiol Rep* **5**, e13244 (2017).

24. Krahl, S. E., Senanayake, S. S. & Handforth, A. Right-sided vagus nerve stimulation reduces generalized seizure severity in rats as effectively as left-sided. *Epilepsy Research* **56**, 1–4 (2003).

25. Navas, M. *et al.* Treatment of refractory epilepsy in adult patients with right-sided vagus nerve stimulation. *Epilepsy Research* **90**, 1–7 (2010).

26. Coote, J. H. & Chauhan, R. A. The sympathetic innervation of the heart: Important new insights. *Autonomic Neuroscience* **199**, 17–23 (2016).

27. Coote, J. H. Myths and realities of the cardiac vagus. *The Journal of Physiology* **591**, 4073–4085 (2013).

28. Palma, J.-A. & Benarroch, E. E. Neural control of the heart: Recent concepts and clinical correlations. *Neurology* **83**, 261–271 (2014).

29. Ross, C. *et al.* Tonic vasomotor control by the rostral ventrolateral medulla: effect of electrical or chemical stimulation of the area containing C1 adrenaline neurons on arterial pressure, heart rate, and plasma catecholamines and vasopressin. *J. Neurosci.* **4**, 474–494 (1984).

30. Dampney, R. *et al.* Central Mechanisms Underlying Short- And Long-Term Regulation Of The Cardiovascular System. *Clin Exp Pharma Physio* **29**, 261–268 (2002).

31. Ross, C. A., Ruggiero, D. A., Joh, T. H., Park, D. H. & Reis, D. J. Adrenaline synthesizing neurons in the rostral ventrolateral medulla: a possible role in tonic vasomotor control. *Brain Research* **273**, 356–361 (1983).

32. Ross, C. A. *et al.* Adrenaline neurons in the rostral ventrolateral medulla innervate thoracic spinal cord: A combined immunocytochemical and retrograde transport demonstration. *Neuroscience Letters* **25**, 257–262 (1981).

33. Guyenet, P. G. & Stornetta, R. L. Rostral ventrolateral medulla, retropontine region and autonomic regulations. *Autonomic Neuroscience* **237**, 102922 (2022).

34. Goodchild, A. K. & Moon, E. A. Maps of cardiovascular and respiratory regions of rat ventral medulla: Focus on the caudal medulla. *Journal of Chemical Neuroanatomy* **38**, 209–221 (2009).

35. Strack, A. M., Sawyer, W. B., Hughes, J. H., Platt, K. B. & Loewy, A. D. A general pattern of CNS innervation of the sympathetic outflow demonstrated by transneuronal pseudorabies viral infections. *Brain Research* **491**, 156–162 (1989).

36. Dampney, R. A. L. *et al.* Medullary and supramedullary mechanisms regulating sympathetic vasomotor tone. *Acta Physiologica Scandinavica* **177**, 209–218 (2003).

37. Sun, M. K. & Guyenet, P. G. GABA-mediated baroreceptor inhibition of reticulospinal neurons. *American Journal of Physiology-Regulatory, Integrative and Comparative Physiology* **249**, R672–R680 (1985).

38. Horiuchi, J. & Dampney, R. A. L. Evidence for tonic disinhibition of RVLM sympathoexcitatory neurons from the caudal pressor area. *Autonomic Neuroscience* **99**, 102–110 (2002).

39. Verberne, A. J. M., Sartor, D. M. & Berke, A. Midline medullary depressor responses are mediated by inhibition of RVLM sympathoexcitatory neurons in rats. *American Journal of Physiology-Regulatory, Integrative and Comparative Physiology* **276**, R1054–R1062 (1999).

40. Barman, S. M., Gebber, G. L. & Orer, H. S. Medullary lateral tegmental field: an important source of basal sympathetic nerve discharge in the cat. *American Journal of Physiology-Regulatory, Integrative and Comparative Physiology* **278**, R995–R1004 (2000).

41. Cravo, S. L. & Morrison, S. F. The caudal ventrolateral medulla is a source of tonic sympathoinhibition. *Brain Research* **621**, 133–136 (1993).

42. Cravo, S. L., Morrison, S. F. & Reis, D. J. Differentiation of two cardiovascular regions within caudal ventrolateral medulla. *American Journal of Physiology-Regulatory, Integrative and Comparative Physiology* **261**, R985–R994 (1991).

43. Schreihofer, A. M. & Guyenet, P. G. Baro-Activated Neurons With Pulse-Modulated Activity in the Rat Caudal Ventrolateral Medulla Express GAD67 mRNA. *Journal of Neurophysiology* **89**, 1265–1277 (2003).

44. Moraes, D. J. A. *et al.* Electrophysiological Properties of Rostral Ventrolateral Medulla Presympathetic Neurons Modulated by the Respiratory Network in Rats. *J. Neurosci.* **33**, 19223–19237 (2013).

45. Lipski, J., Kanjhan, R., Kruszewska, B. & Rong, W. Properties of presympathetic neurones in the rostral ventrolateral medulla in the rat: an intracellular study "in vivo'. *The Journal of Physiology* **490**, 729–744 (1996).

46. Accorsi-Mendonça, D. *et al.* Pacemaking Property of RVLM Presympathetic Neurons. *Front. Physiol.* **7**, (2016).

47. Yuan, H. & Silberstein, S. D. Vagus Nerve and Vagus Nerve Stimulation, a Comprehensive Review: Part I: Headache. *Headache: The Journal of Head and Face Pain* **56**, 71–78 (2016).

48. Sampaio, K. N., Mauad, H., Michael Spyer, K. & Ford, T. W. Chronotropic and dromotropic responses to localized glutamate microinjections in the rat nucleus ambiguus. *Brain Research* **1542**, 93–103 (2014).

49. Cheng, Z. & Powley, T. L. Nucleus ambiguus projections to cardiac ganglia of rat atria: An anterograde tracing study. *J. Comp. Neurol.* **424**, 588–606 (2000).

50. Jones, J. F., Wang, Y. & Jordan, D. Heart rate responses to selective stimulation of cardiac vagal C fibres in anaesthetized cats, rats and rabbits. *The Journal of Physiology* **489**, 203–214 (1995).

51. Wang, J. *et al.* Synaptic and Neurotransmitter Activation of Cardiac Vagal Neurons in the Nucleus Ambiguus. *Annals of the New York Academy of Sciences* **940**, 237–246 (2001).

52. Tan, A. Y. *et al.* Neural Mechanisms of Paroxysmal Atrial Fibrillation and Paroxysmal Atrial Tachycardia in Ambulatory Canines. *Circulation* **118**, 916–925 (2008).

53. Ogawa, M. *et al.* Left Stellate Ganglion and Vagal Nerve Activity and Cardiac Arrhythmias in Ambulatory Dogs With Pacing-Induced Congestive Heart Failure. *Journal of the American College of Cardiology* **50**, 335–343 (2007).

54. Schwartz, P. J., Vanoli, E., Zaza, A. & Zuanetti, G. The effect of antiarrhythmic drugs on life-threatening arrhythmias induced by the interaction between acute myocardial ischemia and sympathetic hyperactivity. *American Heart Journal* **109**, 937–948 (1985).

55. Schwartz, P. J. & Stone, H. L. Left stellectomy in the prevention of ventricular fibrillation caused by acute myocardial ischemia in conscious dogs with anterior myocardial infarction. *Circulation* **62**, 1256–1265 (1980).

56. Takahashi, N. *et al.* Vagal Modulation of Ventricular Tachyarrhythmias Induced by Left Ansae Subclaviae Stimulation in Rabbits. *Jpn Heart J* **39**, 503–511 (1998).

57. Goldstein, R. E. *et al.* Influence of Atropine and of Vagally Mediated Bradycardia on the Occurrence of Ventricular Arrhythmias following Acute Coronary Occlusion in Closed-Chest Dogs. *Circulation* **47**, 1180–1190 (1973).

58. Yu, L. *et al.* Chronic Intermittent Low-Level Stimulation of Tragus Reduces Cardiac Autonomic Remodeling and Ventricular Arrhythmia Inducibility in a Post-Infarction Canine Model. *JACC: Clinical Electrophysiology* **2**, 330–339 (2016).

59. Schlaich, M. P. *et al.* Sympathetic Augmentation in Hypertension: Role of Nerve Firing, Norepinephrine Reuptake, and Angiotensin Neuromodulation. *Hypertension* **43**, 169–175 (2004).

60. Blessing, W. W. & Nalivaiko, E. Regional blood flow and nociceptive stimuli in rabbits: patterning by medullary raphe, not ventrolateral medulla. *The Journal of Physiology* **524**, 279–292 (2000).

61. Jansen, A. S. P., Van Nguyen, X., Karpitskiy, V., Mettenleiter, T. C. & Loewy, A. D. Central Command Neurons of the Sympathetic Nervous System: Basis of the Fight-or-Flight Response. *Science* **270**, 644–646 (1995).

62. Bakris, G. L. *et al.* Baroreflex Activation Therapy provides durable benefit in patients with resistant hypertension: results of long-term follow-up in the Rheos Pivotal Trial. *Journal of the American Society of Hypertension* **6**, 152–158 (2012).

63. De Leeuw, P. W. *et al.* Sustained Reduction of Blood Pressure With Baroreceptor Activation Therapy: Results of the 6-Year Open Follow-Up. *Hypertension* **69**, 836–843 (2017).

64. Bisognano, J. D. *et al.* Baroreflex Activation Therapy Lowers Blood Pressure in Patients With Resistant Hypertension. *Journal of the American College of Cardiology* **58**, 765–773 (2011).

65. Wilks, S. J. *et al.* Non-clinical and Pre-clinical Testing to Demonstrate Safety of the Barostim Neo Electrode for Activation of Carotid Baroreceptors in Chronic Human Implants. *Front. Neurosci.* **11**, 438 (2017).

66. Haïssaguerre, M. *et al.* Spontaneous Initiation of Atrial Fibrillation by Ectopic Beats Originating in the Pulmonary Veins. *N Engl J Med* **339**, 659–666 (1998).

67. Symplicity HTN-1 Investigators. Catheter-Based Renal Sympathetic Denervation for Resistant Hypertension: Durability of Blood Pressure Reduction Out to 24 Months. *Hypertension* **57**, 911–917 (2011).

68. Pokushalov, E. *et al.* A Randomized Comparison of Pulmonary Vein Isolation With Versus Without Concomitant Renal Artery Denervation in Patients With Refractory Symptomatic Atrial Fibrillation and Resistant Hypertension. *Journal of the American College of Cardiology* **60**, 1163–1170 (2012).

69. Lemery, R., Birnie, D., Tang, A. S. L., Green, M. & Gollob, M. Feasibility study of endocardial mapping of ganglionated plexuses during catheter ablation of atrial fibrillation. *Heart Rhythm* **3**, 387–396 (2006).

70. Scherlag, B. J. *et al.* Electrical Stimulation to Identify Neural Elements on the Heart: Their Role in Atrial Fibrillation. *J Interv Card Electrophysiol* **13**, 37–42 (2005).

71. DiBona, G. F. & Kopp, U. C. Neural control of renal function. *Physiological Reviews* **77**, 75–197 (1997).

72. Krum, H. *et al.* Catheter-based renal sympathetic denervation for resistant hypertension: a multicentre safety and proof-of-principle cohort study. *The Lancet* **373**, 1275–1281 (2009).

73. Ukena, C. *et al.* Effects of renal sympathetic denervation on heart rate and atrioventricular conduction in patients with resistant hypertension. *International Journal of Cardiology* **167**, 2846–2851 (2013).

74. Linz, D. *et al.* Renal Sympathetic Denervation Suppresses Postapneic Blood Pressure Rises and Atrial Fibrillation in a Model for Sleep Apnea. *Hypertension* **60**, 172–178 (2012).

75. Zhao, Q. *et al.* Effect of renal sympathetic denervation on the inducibility of atrial fibrillation during rapid atrial pacing. *J Interv Card Electrophysiol* **35**, 119–125 (2012).

76. DiCarlo, L. A. *et al.* Autonomic regulation therapy to enhance myocardial function in heart failure patients: the ANTHEM-HFpEF study. *ESC Heart Failure* **5**, 95–100 (2018).

77. Zannad, F. *et al.* Chronic vagal stimulation for the treatment of low ejection fraction heart failure: results of the NEural Cardiac TherApy foR Heart Failure (NECTAR-HF) randomized controlled trial. *European Heart Journal* **36**, 425–433 (2015).

78. Gold, M. R. *et al.* Vagus Nerve Stimulation for the Treatment of Heart Failure. *Journal of the American College of Cardiology* **68**, 149–158 (2016).

79. Hauptman, P. J. *et al.* Rationale and study design of the INcrease Of Vagal TonE in Heart Failure study: INOVATE-HF. *American Heart Journal* **163**, 954-962.e1 (2012).

80. Schwartz, P. J. *et al.* Long term vagal stimulation in patients with advanced heart failure First experience in man. *European J of Heart Fail* **10**, 884–891 (2008).

81. Shamji, M. F., Westwick, H. J. & Heary, R. F. Complications related to the use of spinal cord stimulation for managing persistent postoperative neuropathic pain after lumbar spinal surgery. *FOC* **39**, E15 (2015).

82. Levy, R. M. Device Complication and Failure Management in Neuromodulation. *Neuromodulation: Technology at the Neural Interface* **16**, 495–502 (2013).

83. Chen, M. *et al.* Non-invasive Autonomic Neuromodulation Is Opening New Landscapes for Cardiovascular Diseases. *Front. Physiol.* **11**, 550578 (2020).

84. Dao, H. H., Lemay, J., Champlain, J. D., deBlois, D. & Moreau, P. Norepinephrine-induced aortic hyperplasia and extracellular matrix deposition are endothelin-dependent: *Journal of Hypertension* **19**, 1965–1973 (2001).

85. Burns, J. *et al.* Relationship Between Central Sympathetic Drive and Magnetic Resonance Imaging–Determined Left Ventricular Mass in Essential Hypertension. *Circulation* **115**, 1999–2005 (2007).

86. Patel, M. Global myocardial hypertrophy in conscious dogs with chronic elevation of plasma norepinephrine levels. *Journal of Molecular and Cellular Cardiology* **21**, 49–61 (1989).

87. Levy, D., Garrison, R. J., Savage, D. D., Kannel, W. B. & Castelli, W. P. Prognostic Implications of Echocardiographically Determined Left Ventricular Mass in the Framingham Heart Study. *N Engl J Med* **322**, 1561–1566 (1990).

88. Haberbusch, M. *et al.* Closed-loop vagus nerve stimulation for heart rate control evaluated in the Langendorff-perfused rabbit heart. *Sci Rep* **12**, 18794 (2022).

89. Romero-Ugalde, H. M. *et al.* Closed-Loop Vagus Nerve Stimulation Based on State Transition Models. *IEEE Trans. Biomed. Eng.* **65**, 1630–1638 (2018).

90. Ugalde, H. R. *et al.* On-off closed-loop control of vagus nerve stimulation for the adaptation of heart rate. in *2014 36th Annual International Conference of the IEEE Engineering in Medicine and Biology Society* 6262–6265 (IEEE, Chicago, IL, 2014). doi:10.1109/EMBC.2014.6945060.

91. Plachta, D. T. T. *et al.* Blood pressure control with selective vagal nerve stimulation and minimal side effects. *J. Neural Eng.* **11**, 036011 (2014).

92. Tosato, M., Yoshida, K., Toft, E., Nekrasas, V. & Struijk, J. J. Closed-loop control of the heart rate by electrical stimulation of the vagus nerve. *Med Bio Eng Comput* **44**, 161–169 (2006).

93. Ardell, J. L. *et al.* Defining the neural fulcrum for chronic vagus nerve stimulation: implications for integrated cardiac control. *The Journal of Physiology* **595**, 6887–6903 (2017).

94. Matsushita, Y. *et al.* TRPC6 is a mechanosensitive channel essential for ultrasound neuromodulation in the mammalian brain. *Proc. Natl. Acad. Sci. U.S.A.* **121**, e2404877121 (2024).

95. Nightingale, K. R. *et al.* Conditionally Increased Acoustic Pressures in Nonfetal Diagnostic Ultrasound Examinations Without Contrast Agents: A Preliminary Assessment. *J of Ultrasound Medicine* **34**, 1–41 (2015).

96. Kubanek, J., Shukla, P., Das, A., Baccus, S. A. & Goodman, M. B. Ultrasound Elicits Behavioral Responses through Mechanical Effects on Neurons and Ion Channels in a Simple Nervous System. *J. Neurosci.* **38**, 3081–3091 (2018).

97. King, R. L., Brown, J. R., Newsome, W. T. & Pauly, K. B. Effective Parameters for Ultrasound-Induced In Vivo Neurostimulation. *Ultrasound in Medicine & Biology* **39**, 312–331 (2013).

98. Iversen, M. M. *et al.* Low-intensity ultrasound activates vestibular otolith organs through acoustic radiation force. *The Journal of the Acoustical Society of America* **141**, 4209–4219 (2017).

99. Cracchiolo, M. *et al.* Bioelectronic medicine for the autonomic nervous system: clinical applications and perspectives. *J. Neural Eng.* **18**, 041002 (2021).

100. Pavlov, V. A. Cholinergic modulation of inflammation. *Int J Clin Exp Med* **1**, 203–212 (2008).

101. Brooks, V. L. & Osborn, J. W. Hormonal-sympathetic interactions in long-term regulation of arterial pressure: an hypothesis. *American Journal of Physiology-Regulatory, Integrative and Comparative Physiology* **268**, R1343–R1358 (1995).

102. Guyenet, P. G. The sympathetic control of blood pressure. *Nat Rev Neurosci* **7**, 335–346 (2006).

103. Dean, C., Seagard, J. L., Hopp, F. A. & Kampine, J. P. Differential control of sympathetic activity to kidney and skeletal muscle by ventral medullary neurons. *Journal of the Autonomic Nervous System* **37**, 1–10 (1992).

104. Ding, Z.-Q., Li, Y.-W., Wesselingh, S. L. & Blessing, W. W. Transneuronal labelling of neurons in rabbit brain after injection of Herpes simplex virus type 1 into the renal nerve. *Journal of the Autonomic Nervous System* **42**, 23–31 (1993).

105. Carrive, P. & Bandler, R. Viscerotopic organization of neurons subserving hypotensive reactions within the midbrain periaqueductal grey: a correlative functional and anatomical study. *Brain Research* **541**, 206–215 (1991).

106. Pereira, E. A. C. *et al.* Sustained reduction of hypertension by deep brain stimulation. *Journal of Clinical Neuroscience* **17**, 124–127 (2010).

107. Patel, N. K. *et al.* Deep brain stimulation relieves refractory hypertension. *Neurology* **76**, 405–407 (2011).

108. Li, D. *et al.* Low-intensity focused ultrasound stimulation treatment decreases blood pressure in spontaneously hypertensive rats. *IEEE Trans. Biomed. Eng.* 1–1 (2020) doi:10.1109/TBME.2020.2975279.

109. Cao, F. *et al.* Non-Invasive Ultrasound Modulation of Solitary Tract Nucleus Exerts a Sustainable Antihypertensive Effect in Spontaneously Hypertensive Rats. *IEEE Trans. Biomed. Eng.* **70**, 1869–1878 (2023).